ORIGINAL PAPER

Engineering geology and future stability of the El Risco landslide, NW-Gran Canaria, Spain

Marc-Antoine Longpré · Rodrigo del Potro ·
Valentin R. Troll · Graeme R. Nicoll

Abstract A 200 m long segment of the only main road in NW-Gran Canaria is built on landslide deposits near the village of El Risco. Structural mapping and analysis of the topography reveal that the N–S striking landslide head scarp is the upper part of a sub-circular failure surface. The southern side of the landslide is delimited by a much older E–W strike-slip fault. Prior to pavement resurfacing in 2006, cracks in the road tarmac at the northern and southern sides of the landslide suggested ongoing creep movement. Slope stability analyses suggest that peak ground acceleration (PGA) was the most likely trigger for the initial failure.

Keywords Landslide · Road infra-structures · Basaltic lavas · Slope stability analyses · Peak ground acceleration

Résumé La seule route majeure desservant le nord-ouest de Grande Canarie est construite sur les dépôts d'un glissement de terrain sur une longueur de 200 m, près du village d'El Risco. Une cartographie structurale et l'analyse de la topographie ont révélé que l'escarpement de tête, de direction N–S, constitue la partie supérieure d'une surface de rupture sub-circulaire. La partie sud du glissement est délimitée par une faille orientée E–W. Avant l'application d'une nouvelle couche d'asphalte en 2006, des fissures dans la chaussée coïncidaient avec les limites du glissement et auraient pu correspondre à un lent mouvement de fluage en cours. Les analyses de stabilité des pentes indiquent qu'une accélération séismique est la cause la plus probable de la rupture initiale.

Mots clés Glissement de terrain · Infrastructures · Laves basaltiques · Analyses de stabilité de pente · Accélération séismique

M.-A. Longpré (✉) · V. R. Troll · G. R. Nicoll
Department of Geology, Trinity College Dublin,
Dublin 2, Ireland
e-mail: longprem@tcd.ie

R. del Potro
Department of Environmental Science, Lancaster University,
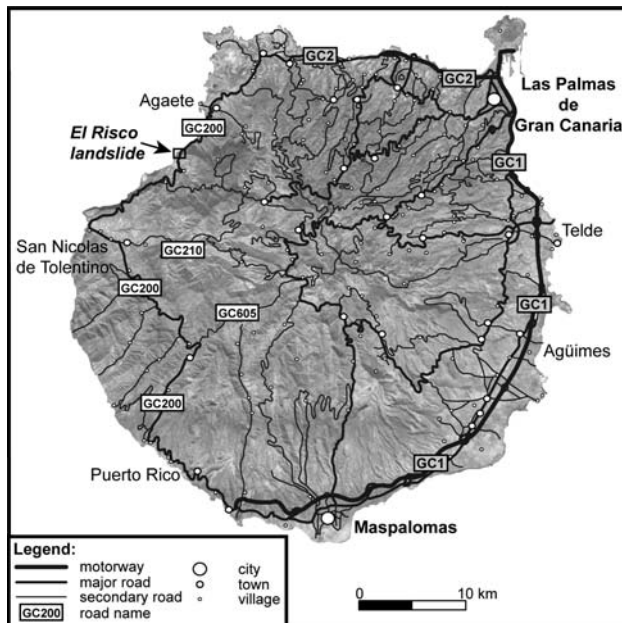Lancaster, UK

Introduction

The coastal regions of volcanic ocean islands are often characterised by steep and unstable slopes, which pose considerable challenges for road engineering. Transportation infra-structure needs to accommodate heavier traffic loads due to the dense and increasing population: there are 610 inhabitants per km^2 in Mauritius, 520 in Gran Canaria, 420 in Tenerife and 315 in La Réunion (United Nations 2004; Instituto Nacional de Estadística 2006). Careful planning by engineers is required to minimise road construction costs and optimise road endurance with minimum maintenance. Complex measures and designs, such as long tunnels excavated to bypass steep topography, are efficient but very cost intensive. Where traffic flows are smaller and budgets for infra-structure low, the construction of winding and often narrow roads is a cost-effective alternative.

In Gran Canaria, where the population of 807,000 is increased by some 3 million tourists who visit each year (Instituto Nacional de Estadística 2006), only one direct route (road GC-200) links the villages of the west, such as San Nicolás de Tolentino and Mogán, to the urban centres of Las Palmas and Maspalomas in the north and the south of the island (Fig. 1). Other roads through the mountainous centre of the island, such as GC-210, are extremely winding and narrow with some segments only single-track.

Fig. 1 Satellite image of Gran Canaria showing the location of roads, cities and villages. The *black rectangle* (enlarged in Fig. 2) corresponds to the location of the El Risco landslide

Located on the edge of the cliff-dominated western coastline, the GC-200 is slightly less winding and narrow, but is heavily used by both local and commercial traffic as well as by tourists wanting to appreciate the spectacular scenery. A 200 m long section of this road, located 2 km north of the village of El Risco, crosses the El Risco landslide (Figs. 2, 3). A power line and a dirt track that descend to the coast also partly cross the landslide.

Based on a combination of fieldwork, examination of aerial and oblique photographs and slope stability analyses, the paper presents a detailed study of the El Risco landslide. Generalised parameters are used to consider the mechanisms and causes of the failure and to evaluate the present-day stability and the risk of future instability.

Background geology

In north–west Gran Canaria, the Miocene shield-building basalts, the oldest sub-aerial rocks of the island ($\geq$14 Ma), dominate the landscape (McDougall and Schmincke 1977; Bogaard and Schmincke 1998). These lava flows, which dip slightly to the east, are moderately altered, with many feldspar phenocrysts replaced by zeolite and clay minerals. Moreover, abundant calcite, zeolites and gypsum occur in cracks, vesicles and voids whilst part of the ferromagnesian minerals and the matrix is replaced by alteration minerals such as serpentine and epidote.

A 19 km wide coastal re-entrant, cutting into the basalts of north–west Gran Canaria, represents the trace of a huge Miocene landslide, with the deposits extending some 20 km off-shore (Funck and Schmincke 1998). Erosion and smaller slope failures within this coastal embayment, including the study site, maintain the cliff-dominated shore, characterised by slopes of 45° and steeper. Several faults are reported from the region, either concentric or radial to the Miocene central Tejeda caldera (Schmincke 1967; Troll et al. 2002).

Dykes of variable composition, mostly radial to the Tejeda caldera, are frequently encountered in the region (Schmincke 1976). Five distinct dykes that can be traced over several hundred metres crop out in the vicinity of the El Risco landslide (Figs. 2, 3) although not identified within the landslide deposits. Two dykes (P1 and P2) of phonolitic composition are the most prominent intrusive features. Both are sub-vertical, have a broad north–west trend, a width of about 1.5 m and a distinctive pinkish colour. A narrower phonolitic dyke (P3), trending broadly west, is encountered at the coast and is cut by P1. Two basaltic dykes (B1 and B2) are observed. B1 is a massive $\sim$0.5 m wide dyke and trends broadly north; it is cut by both P1 and P2. B2 is altered and displays an olivine-rich core; it generally trends north but is irregular with several offshoots. It is cut by P2, but its relationship with P1 cannot be determined on the basis of present exposure.

A horizontal offset of $\sim$55 m is observed for three dykes (P2, B1, B2, see Fig. 2) whilst no offset of P1 is obvious although a 200 m long segment of this dyke is missing and probably was removed or covered by the landslide. The observed displacement is due to an E–W strike-slip (sinistral) fault located at the southern boundary of the study site and characterised by a well-developed and solidified fault breccia. The attitude of the fault plane, exposed in three main areas, is 085/65 N. In one site below the road, a fault plane section (2 m high, $\sim$30 m long) contains intense calcite and zeolite mineralisation. Slickensides found in two locations (Fig. 2) plunge 2–4° to 264°(S84°W), indicating strike-slip movement. The fault extends beyond the landslide area inland for at least 200 m, with small vertical displacements estimated to be up to 15–20 m down-dip to the north. These observations suggest that this fault is older than the landslide and probably related to Miocene cyclic activity of the Tejeda magmatic system (cf. Troll et al. 2002).

The El Risco landslide

The El Risco landslide is some 45,000 m^2, extending between 75 and 275 m above sea level. Field observations and cross sections show it to be abruptly delimited to the

Fig. 2 Topographic map of the El Risco landslide and surroundings. Locations of photographs (Fig. 3) and topographic profiles (Fig. 4) are indicated
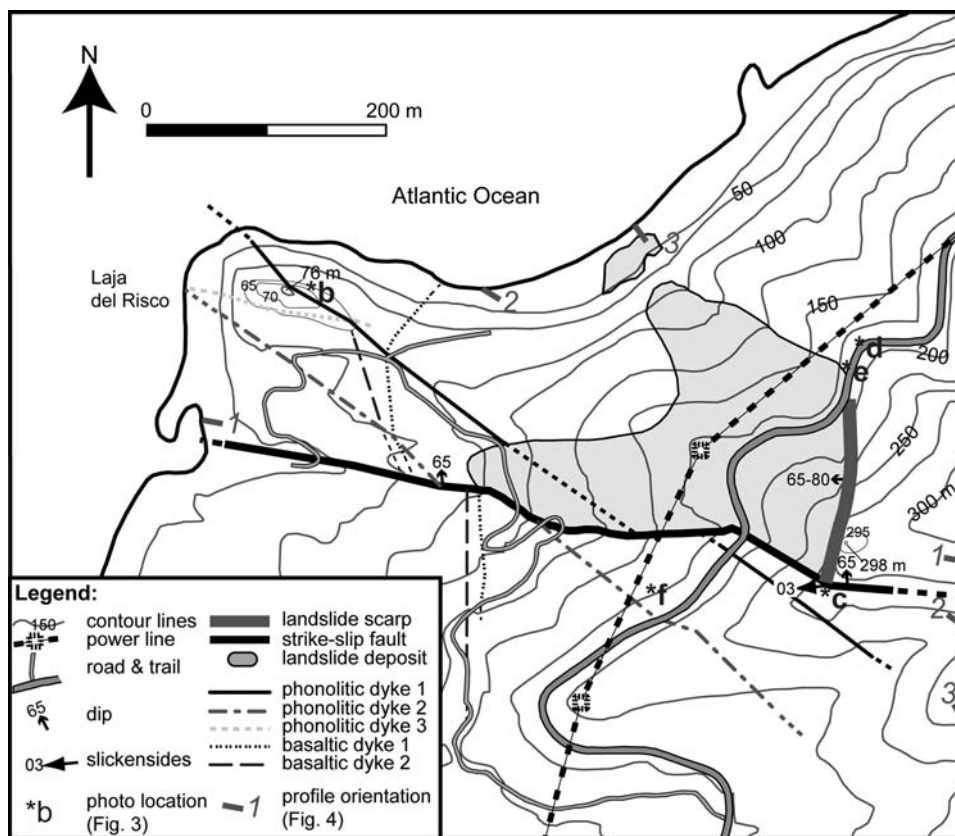
east by a 65°–80° head scarp with a weakly arcuate N–S trend (Figs. 2, 3, 4). The head scarp is considered to represent the exposed prolongation of a sub-circular failure surface underlying the displaced rock mass. The surface of the head scarp is irregular and rough and neither fault breccia nor slickensides were observed. No trace of the failure surface is exposed below the road to the north. To the south, however, the head scarp terminates at right angles to the older strike-slip fault (Fig. 2). Whilst the older strike-slip fault did not act as a primary failure surface, it appears to have provided a constraint to the southern extent of the landslide.

The upper part of the failed mass is composed of detached blocks that kept their relative stratigraphic position but were rotated backwards (Fig. 3f). In contrast to the regional basaltic lavas dipping <15°E, the displaced flows have dips of 20°E–25°E towards the landslide head which steepen to 45°E in the middle part, just below the road, before shallowing to 10°E towards the toe. Following Varnes (1978), the El Risco landslide would be described as a rotational slump. However, the two lobes of landslide deposits forming the landslide toe consist of disaggregated blocks which were probably emplaced at higher velocities as a small-scale debris avalanche.

Although the toe of the rotational plane is obscured by the landslip material, field observations and analysis of topographic profiles suggest that the lower part of the sub-circular failure surface is located slightly above 125–135 m asl (Fig. 4b). Pre-failure topography was inferred by comparing topographic patterns encountered inside and outside the landslide area. This suggests that a significant volume of deposits from the northern arm of the slide may have been transported to the beach where it was probably rapidly eroded by wave action (Fig. 4c). From the assumed pre-failure topography, the inferred position of the failure surface and the landslide area, a volume of around one million cubic metres may have been displaced.

During the spring 2005 fieldwork, cracks in the road tarmac were observed along the northern and southern edges of the slide (Fig. 3d), suggesting ongoing creep. The GC-200 road was subsequently resurfaced in 2006.

Slope stability analyses

Back-analysis based on 2D homogeneous limit equilibrium models (LEM) was undertaken following Bishop's modified method (Bishop 1955). The non-circular Spencer (1967) and Jambu (1957) methods were also tested. All three methodologies produced very similar stability and geometrical values for the El Risco landslide; therefore, Bishop's modified method was retained for simplicity. It

Fig. 3 Images of the El Risco landslide with the affected infra-structure and the major geological features labelled. **a** Satellite image of the El Risco landslide, courtesy of GRAFCAN. **b** Panorama of the landslide as seen from the west, and **c** from the north. **d** Photo (taken in April 2005) of cracks in road GC-200 coincident with the northern landslide edge. **e** View from the east. **f** Photo mosaic taken from the south showing rotation of landslide blocks

was assumed that prior to failure the site could be con-sidered as a well-defined block delimited by the strike-slip fault to the south and a fluvial valley to the north; potential regional/local vertical discontinuities were not considered in the models. The main source of uncertainty in such slope stability models arises in the values of the parameters characterising the slope conditions at the time of failure; essentially the rock-mass strength parameters, the water table conditions, the original topography and failure geometry. A combination of parameter sensitivity analyses and slope instability back-analyses were used to assess the values.

Rock-mass strength

The rock mass involved in the El Risco landslide is entirely composed of hydrothermally altered, partly scoriaceous

basaltic lava flows of Miocene age. The rock mass strength parameter values used in the study are shown in Table 1. According to the Geotechnical Strength Index (GSI) pro-posed by Hoek et al. (1995), the rock mass is BLOCKY and the condition of the joints is FAIR, giving a minimum GSI of 45. Using Watters and Delahaut's (1995) scale (0—no alteration to 4—completely altered to clay) the degree of alteration corresponds to a value of 2. In the first model (i), φ' values ranging from 20° to 40° and c' values of 0 to 300 kPa were used based on other studies (Watters et al. 2000; Concha-Dimas 2004; Thomas et al. 2004; Zimbelman et al. 2004; Apuani et al. 2005) and field observations. Based on preliminary results from the first model, a friction angle of 30° was assumed for the second model (ii) and a cohesion value of zero was taken to represent residual strength conditions. Unit weight (γ) values of 19 to 28 kN/m^3, spanning most volcanic materials, were used to assess the effect of material density on slope stability for model (i) and,
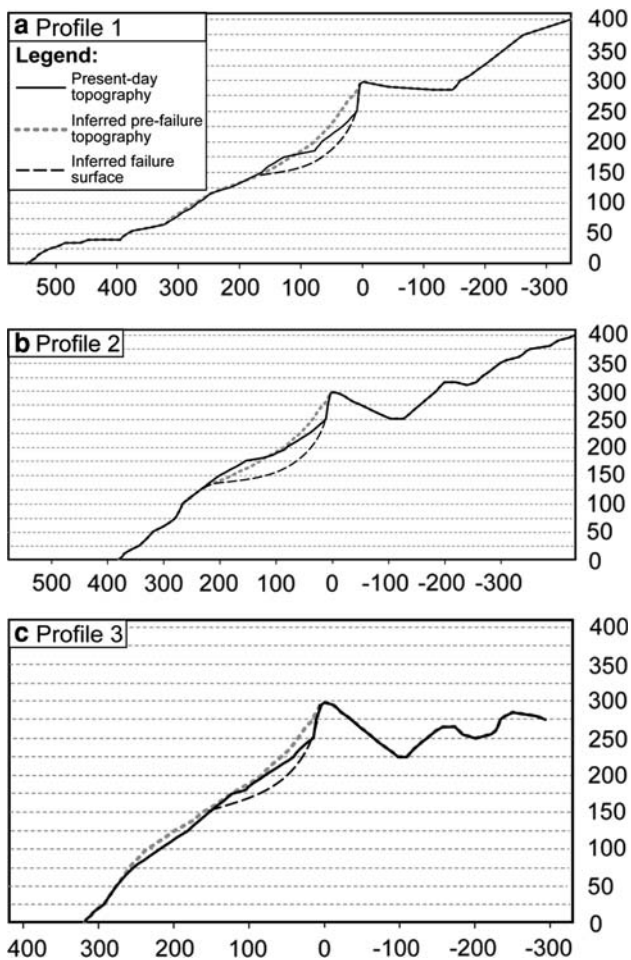
Fig. 4 Current topography, inferred pre-failure topography and inferred failure surface geometry for **a** profile 1, **b** profile 2 and **c** profile 3 of Fig. 2

given its negligible effect on the stability analyses, a representative value of 24 kN/ m^3 was taken for (ii).

Water table conditions

Little is known of the ground water conditions at El Risco, due to the lack of data on rock permeability and precipitation and the absence of wells in the area. However, the observed basaltic lava flows are generally fractured with

Table 1 Values of the parameters used in the stability models

Model	Unit weight, Y (kN/m^3)	Friction angle, φ' (°)	Cohesion, c' (kPa)	Peak ground acceleration (g)	Water table height (%)
(i)	19–28	20–40	0–300	0–0.35	0–100
(ii)	24	30	0	0–0.3	0–100

their top and bottom breccias apparently forming horizons of increased permeability (Cabrera and Custodio 2004). In the absence of clay-rich units, perched water tables are unlikely to develop in the area. The proximity of the slope to the sea, the elevation of the failure surface above sea level and the existence of lower land behind the scarp indicate generally dry conditions are likely to have pertained on the upper sector of the slope, where the failure developed. Nevertheless, different ground water table elevations were considered, from 0 to 100% in 10% increments. Following Dupuit–Forchheimer theory (Bear 1972), the water table model was simplified to an ellipse with the major and minor axis lengths equal to the modelled slope width and maximum water table height (Fig. 5a).

Peak ground accelerations (PGA)

Ground accelerations resulting from seismic events are a very common trigger for rock slope instabilities (Keefer 2002). Most significant to the present study is seismic activity related to an off-shore strike-slip fault oriented NNE-SSW and located between the islands of Gran Canaria and Tenerife, 30 km from the El Risco site. This system has been active historically, with recorded magnitudes of up to 5.2 (Mezcua et al. 1992) whilst palaeoearthquake investigations indicate maximum values of $M = 6.8$ (González de Vallejo et al. 2003). In addition, lower magnitude earthquakes (generally $M < 3$) have been repeatedly reported for all the Canary Islands (Instituto Geográfico Nacional data 1993–2004). From this, two seismic scenarios were modelled: a deep (15–50 km) $\sim$M7 earthquake at a distance of $\sim$30 km and a shallow (<20 km) $\sim$M3 earthquake at a distance of $\sim$10 km. Following a number of empirical solutions which relate peak ground acceleration (PGA) to event magnitude and distance from source (Okamoto 1984; Joyner and Boore 1993; Campbell and Bozorgnia 1994), PGA values of up to 0.35 g were chosen (Fig. 5b). This is consistent with other studies (e.g. Voight et al. 1983; Hürlimann et al. 2000).
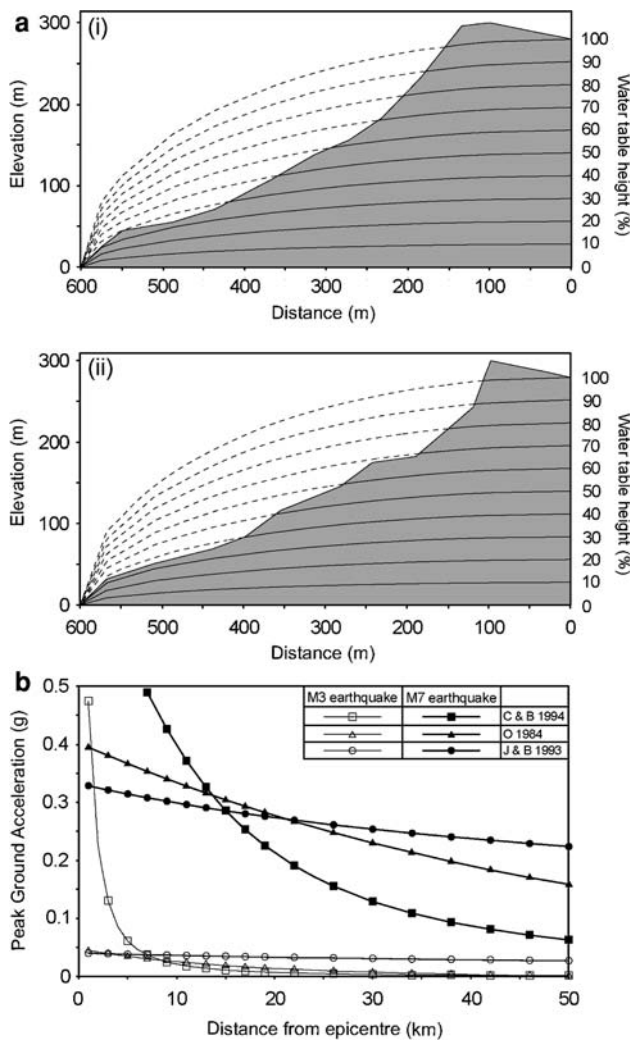
Results

Pre-failure conditions

The parameter sensitivity tests indicate that small variations in rock mass strength parameters significantly affect the factor of safety (Fig. 6a).

The depth and geometry of a circular failure plane is mainly controlled by the cohesion of the material (c'). The results of the analysis of the inferred pre-failure and present-day slopes, following the work of Wesley and
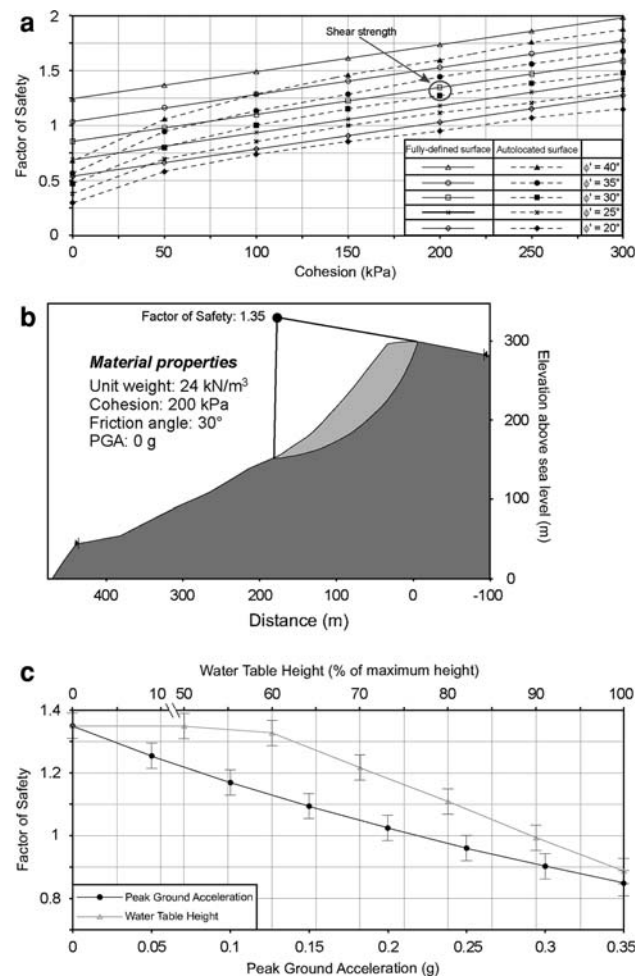
Fig. 5 a (i) Pre- and (ii) post-failure water table geometries used in the stability models, following the Dupuit–Forchheimer theory. b Peak ground acceleration as a function of earthquake magnitude and distance to the epicentre using the empirical equations of Campbell and Bozorgnia (1994), Joyner and Boore (1993) and Okamoto (1994)

Fig. 6 Results for model (i). a Factor of safety as a function of material cohesion for different angles of internal friction, for models with a user-specified failure surface (fully-defined) and models with a non-specified failure surface (autolocated), following the methodology proposed by Wesley and Leelaratnam (2001). b Calculated initial failure surface. c Comparison of the decrease in the factor of safety induced by peak ground accelerations and increasing water table heights. The error bars represent the variation given by the range of material unit weights used in the calculations

Leelaratnam (2001), show that a cohesion value of ~200 kPa and an angle of internal friction of ~30° best reproduce the observed/inferred failure surface (Fig. 6b). Using these values under dry conditions, an initial, static factor of safety of 1.349 was obtained.

The modelling indicated that the initial factor of safety is not affected by water table heights of up to 60% of the total maximum height (Fig. 5a, 6b). Water table heights between 60 and 100% of the total maximum height result in a gradually reduced factor of safety, to below 1 for values above ~90%.

Peak ground accelerations have a more significant effect on the factor of safety; a PGA value of ~0.22 g being sufficient to decrease the factor of safety to a value of 1 (Fig. 6c).

Current stability of the failed mass

Using the residual cohesion value of 0 kPa and an angle of internal friction of 30°, the model showed a factor of safety of 1.252 for the present-day slope under dry conditions (Fig. 7a). As with model (i), the factor of safety remains constant with water table heights up to 50% of the total maximum height. A sharp decrease in the factor of safety is observed with higher values, with a value of ~65% resulting in a factor of safety of 1 (Fig. 7b). The relationship between the factor of safety and peak ground acceleration established in model (i) also pertains for model (ii), although the factor of safety is reduced to 1 with a peak ground acceleration of ~0.1 g (Fig. 7b).
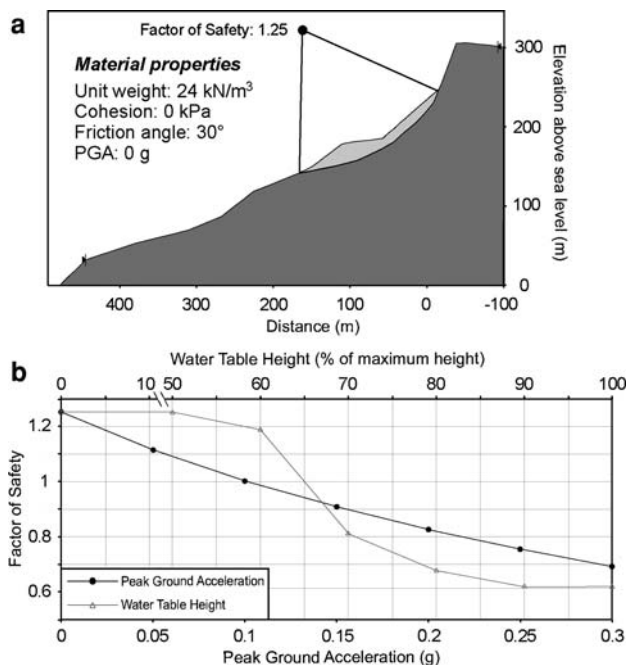
Fig. 7 Results for model (ii). **a** Calculation of failed mass geometry. **b** Comparison of the decrease in the factor of safety induced by peak ground accelerations and increasing water table heights for the present state of the slope

Discussion and conclusion

The El Risco landslide, located within the trace of a giant Miocene landslide in north-western Gran Canaria, is a $\sim 10^6$ m^3 rotational slump and covers an area of $\sim 45,000$ m^2. The failed mass consists of moderately altered, partly scoriaceous basaltic lava flows. Before failure, the mass was bounded by a strike-slip fault to the south and an eroded valley to the north, in a region where north–south and east–west trending fractures are common and thought to be related to the influence of Miocene volcanic edifices. The failure, possibly recent although older than the road, occurred along a sub-circular, N–S striking failure surface, aided and constrained by the pre-existing E–W strike-slip fault.

Slope stability analyses were undertaken, based on the following assumptions:

(1) the failed block was semi-detached before failure; and
(2) the only three potential factors to have influenced slope failure were

    (a) the low shear-strength of the material,
    (b) an increase of pore water pressures during peak precipitation events and
    (c) peak ground accelerations caused by seismicity.

The modelling suggests that high pore water pressures alone were unlikely to have caused initial failure while peak ground accelerations equal to or greater than 0.22 g may have been sufficient. Using empirical equations (Okamoto 1984; Joyner and Boore 1993; Campbell and Bozorgnia 1994), it was found that such peak ground accelerations could have been generated by a seismic event $\geq$M7 along the sub-marine strike-slip fault, located 30 km off-shore, which could have taken place in the geological past (Gonzalez de Vallejo et al. 2003). With an earthquake epicentre within a 10 km radius, a $\geq$M6 event would have been required, suggesting that the smaller and more common $\sim$M3 seismic shocks are unlikely to have triggered the initial failure.

Modelling the current slope stability conditions suggests a factor of safety of 1.252. This is consistent with the ongoing creep of the landslide mass indicated by cracking of the road tarmac at the northern and southern extremities. The calculations show that a water table height of 65% of the total maximum height would create pore pressures high enough to destabilise the slope. With a 10% safety margin, a failure could be triggered if the water table rises to some 165 m above sea level at a location directly beneath the landslide head. This situation is difficult to envisage at the El Risco site, unless the permeability of horizons between individual lava flows has been overestimated.

It was calculated that a seismic event generating a peak ground acceleration of only 0.1 g at the El Risco site would cause further failure of the landslide mass under dry conditions. Applying a 10% safety buffer indicates a threshold PGA value of 0.09 g, equivalent to a $\geq$M5 earthquake along the NNE-SSW sub-marine fault 30 km west of El Risco or a $\geq$M4.5 earthquake located within a 10 km radius. Considering that at least two $\geq$M5 seismic events occurred historically at the sub-marine fault between Gran Canaria and Tenerife and a M3–4 earthquake occurred in the vicinity of the El Risco site as recently as 1999 (Instituto Geográfico Nacional data 1993–2004), both of these scenarios are likely to occur again in the foreseeable future.

Other secondary factors that could contribute to future failure of the El Risco landslide include

(a) further alteration of the material by weathering and erosion of the landslide toe
(b) anthropogenic activity, such as the removal of landslide material during road construction and the vibrations caused by traffic.

It should also be remembered that Gran Canaria is a volcanic island and therefore may be affected by future volcanic activity and accompanying seismicity. Such activity would most likely take place in the north–east of the island and, although there is no indication that it is imminent in the near future, it could potentially contribute to accelerated slope movement at El Risco.

It is of note that other sections of the GC-200 road along Gran Canaria's north–western coastline share the same characteristics as those of the El Risco landslide site, hence nearby slopes might respond in a similar way to an external triggering event.

It is recommended that monitoring is undertaken, including regular observation as well as the installation of monitoring instruments (inclinometers and piezometers) to determine the precise displacement rates and hydrological conditions in the area. In addition, in view of the hazards presented by re-activation of the El Risco landslide, the costs of periodical road stabilisation should be estimated and compared to that of the construction of a new road section bypassing it.

References

Apuani T, Corazzato C, Cancelli A, Tibaldi A (2005) Physical and mechanical properties of rock masses at Stromboli: a dataset for volcano instability evaluation. Bull Eng Geol Environ 64(4):419–431

Bishop AW (1955) The use of slip circles in the stability analysis of slopes. Géotechnique 5:7–17

Bear J (1972) Dynamics of fluids in porous media. Environmental Science Series. American Elsevier, New York, 764 pp

Bogaard Pvd, Schmincke H-U (1998) Chronostratigraphy of Gran Canaria. In: Weaver PPE, Schmincke H-U, Firth JV, Duffield W (eds) Proceedings of the ocean drilling program, scientific results 157. Ocean drilling program, College Station, TX, pp 127–140

Cabrera MC, Custodio E (2004) Groundwater flow in a volcanic-sedimentary coastal aquifer: Telde area, Gran canaria, Canary Islands, Spain. Hydrogeol. J 12(3):305–320

Campbell KW, Bozorgnia Y (1994) Near-source attenuation of peak horizontal acceleration from worldwide accelerograms recorded from 1957 to 1993. In: Institute EER (ed), 5th US National Conference on Earthquake Engineering, Berkeley, California, pp 283–292

Concha-Dimas A (2004) Numerical modelling in understanding catastrophic collapse at Pico de Orizaba, Mexico. PhD Thesis, University of Nevada, Reno

Funck T, Schmincke H-U (1998) Growth and destruction of Gran Canaria deduced from seismic reflection and bathymetric data. J Geophys Res 103:15393–15407

González de Vallejo LI, Capote R, Cabrera L, Insua JM, Acosta J (2003) Paleoearthquake evidence in Tenerife (Canary Islands) and possible seismotectonic sources. Marine Geophys Res 24(1–2):149–160

Hoek E, Kaiser PK, Bawden WF (1995) Support of underground excavations in hard rock. Balkema, Rotterdam

Hürlimann M, Marti J, Ledesma A (2000) Mechanical relationship between catastrophic volcanic landslides and caldera collapses. Geophys Res Lett 27(16):2393–2396

Instituto Nacional de Estadística, Poblaciones referidas al 1 de enero de 2006 por Islas y sexo. http://www.ine.es/inebase/cgi/axi?AXIS_PATH=/inebase/temas/t20/e260/a2006/l0/&FILE_AXIS=is01.px&CGI_DEFAULT=/inebase/temas/cgi.opt&COMANDO=SELECCION&CGI_URL=/inebase/cgi/. Retrieved 15 Jan 2007

Instituto Geográfico Nacional, Ministerio de Fomento, Información sísmica, boletines definitivos de sismos próximos (1993–2004). http://www.fomento.es/MFOM/LANG_CASTELLANO/DIRECCIONES_GENERALES/INSTITUTO_GEOGRAFICO/Geofisica/sismologia/informacionsis/default.htm. Retrieved 15 Jan 2007

Janbu N (1957) Earth pressure and bearing capacity by generalized procedure of slices. In: Proceedings of the fourth international conference on soil mechanics, pp 207–212

Joyner WB, Boore DM (1993) Methods for regression analysis of strong-motion data. Bull Seismol Soc Am 83(2):469–487

Keefer DK (2002) Investigating landslides caused by earthquakes - a historical review. Surv Geophy 23(6):473–510

McDougall I, Schmincke H-U (1977) Geochronology of Gran Canaria, Canary Islands: age of shield building volcanism and other magmatic phases. Bull Volcanol 40(1):57–77

Mezcua J, Burforn E, Udías A, Rueda J (1992) Seismotectonics of the Canary Islands. Tectonophys 208:447–452

Okamoto S (1984) Introduction to earthquake engineering. University of Tokyo Press, pp 629

Population Division of the Department of Economic and Social Affairs of the United Nations Secretariat, World Population Prospects: The 2004 Revision and World Urbanization Prospects: The 2003 Revision. http://esa.un.org/unpp. Retrieved 15 Jan 2007

Schmincke H-U (1967) Cone sheet swarm, resurgence of Tejeda caldera, and the early geologic history of Gran Canaria. Bull Volcanol 31:153–162

Schmincke H-U (1976) The geology of the Canary Islands. In: Kunkel G (eds) Ecology and biogeography in the Canary Islands. The Hague, Netherlands, Junk B V, pp 67–184

Spencer E (1967) Method of analysis of the stability of embankments assuming parallel interslices forces. Géotechnique 17(1):11–26

Thomas ME, Petford N, Bromhead EN (2004) Volcanic rock-mass properties from Snowdonia and Tenerife: implications for volcano edifice strength. J Geol Soc 161:939–9046

Troll V R, Walter T R, Schmincke H-U (2002) Cyclic caldera collapse: piston or piecemeal subsidence? Field and experimental evidence. Geol 30:135–138

Varnes DJ (1978) Slope movements types and processes. Landslides Analysis and Control Transportation Research Board. National Academy of Sciences Special Report 176. Chapter 2, pp 11–33

Voight B, Janda RJ, Glicken H, Douglass PM (1983) Nature and mechanics of the Mount St-Helens rockslide-avalanche of 18 May 1980. Geotechnique 33(3):243–273

Watters RJ, Delahaut WD (1995) Effect of argillic alteration on rock mass stability. In: Haneberg WC, Anderson SA (eds) Clay and shale slope instability. reviews in engineering geology. Geological Society of America, Boulder, CO, pp 139–150

Watters RJ, Zimbelman DR, Bowman SD, Crowley JK (2000) Rock mass strength assessment and significance to edifice stability, Mount Rainier and Mount Hood, Cascade Range volcanoes. Pure Appl Geophys 157(6–8):957–976

Wesley LD, Leelaratnam V (2001) Shear strength parameters from back-analysis of single slips. Geotech 51(4):373–374

Zimbelman DR, Watters RJ, Firth IR, Breit GN, Carrasco-Nunez G (2004) Stratovolcano stability assessment methods and results from Citlaltepetl, Mexico. Bull Volcanol 66(1):66–79